Modelling of Multibody Marine Systems with Application to Wave-Energy Devices

Mícheál Ó'Catháin[1], Bernt J. Leira[2] and John V. Ringwood[3]

[1] Dept. Electronic Engineering, NUIM, IRELAND
E-mail: ocathain@stud.ntnu.no

[2]Dept. Marine Technology, NTNU, NORWAY
E-mail: Bernt.Leira@marin.ntnu.no

[3] Dept. Electronic Engineering, NUIM, IRELAND
E-mail: John.Ringwood@eeng.nuim.ie

Abstract

Time-domain modelling of wave-energy devices is important. This is due to the need for information on the device's transient response characteristics; even when linear potential theory is assumed when modelling hydrodynamic loads, significant non-linearities may be present in the system due to the power-take off (PTO), mooring, and control subsystems. In this paper, an approach for modelling multibody marine systems is presented. The Newton-Euler equations with eliminated constraints (NE-EC) are utilised to capture the rigid body dynamics of the constrained multibody system. This results in the convenient integration of active loads (as opposed to interbody *constraint* forces) acting on the multibody system. In this paper, the active loads considered are: hydrodynamic, PTO, and mooring loads.
Keywords: multibody, time-domain, Newton-Euler equations, modelling for control

1 Introduction

Research on modelling of multibody marine systems has been conducted before. In the field of ocean wave-energy, early contributions were made by [1–5]. More recently, Kraemer [6] describes a method to simulate the motions of hinged-barge systems in regular seas. Rigid connections between bodies are considered, and are modelled with a force-based approach, using free-body diagrams. The hydrodynamic modelling of the method involves the use of scaled data from a vessel which is geometrically similar to that of the individual barges; no hydrodynamic coupling between barges is considered, and radiation coefficients for a given frequency are used to give motions of the system in monochromatic waves at that same frequency. Mooring and PTO subsystems are modelled as linear damper-springs, and the viscous damping force due to vortex shedding around a submerged damper plate is modelled as a quadratic damping expression proportional to a drag coefficient.

Additionally, Berntsen [7] developed models, of both high and reduced complexity, of a futuristic offshore fish-farm concept consisting of five interconnected semi-submersible modules. A force-based approach was used to describe the connectors between the modules, which were modelled as damper-spring elements at each of the four connecting corners of the modules; hence rigid connections between modules were not considered. Hydrodynamic data from a vessel geometrically similar to each of the semi-submersible modules was used with hydrodynamic coupling between modules neglected. No wave-frequency forces were considered, *i.e.*, radiation-induced loads; only slowly-varying environmental loads were modelled. A comprehensive model of a turret mounted spread-mooring subsystem was applied, with internal elasticity together with external viscous drag and hydrostatic loads captured via a finite element approach. Additionally a thruster and hydrofoil acted as actuators to position the system as desired in cooperation with the mooring system. A number of controllers were developed, with and without the use of state-estimators, with the objective of reducing the maximum loading on the lines.

This paper proposes an approach to multibody marine system modelling which addresses a number of outstanding issues from the previous work just described. The issues addressed are:

- Convenient integration of hydrodynamic data from potential theory programs dedicated to a specific multibody geometry, rather than use of scaled data from a geometrically similar single vessel.
- Hydrodynamic coupling between connected bodies
- Implementation of recent research into the time-domain models of radiation-induced loads

In addition, kinematic issues of PTO placement are treated, with reconfiguration possible via a change in geometrical parameters. The modelling approach is experimentally validated. The paper is organised as follows: the next section, Section 2 describes the general method, considering rigid-body dynamics as well as hydrodynamics. An example is presented in Section 3, providing an specific application of the modelling method, *i.e.*, a two-body line-absorber wave-energy device; additional modelling of PTO, hinge friction and mooring subsystems is considered in this section. Experimental validation of the previous application example is treated in Section 4. Section 5 provides some concluding

remarks on the implications of the results presented herein, as well as suggestions for further work.

2 Dynamics

2.1 Constraints

For a free floating (unconstrained) marine vessel, the number of degrees of freedom is equal to 6. The generalised Cartesian coordinates recommended by [8] for such a free floating vessel are independent, i.e., $\boldsymbol{\eta} = [x, y, z, \phi, \theta, \psi]^\top$. If we introduce constraints between the bodies in a multibody system, the number of degrees of freedom (DOF) of the system is reduced. Some of the Cartesian (generalised) coordinates thus become redundant, so that it is possible to describe the motion of each body in the system using fewer (independent) coordinates. In other words, the number of independent coordinates is reduced due to the constraints. The *independent coordinates* of a multibody systems are also called the system *degrees of freedom* [9]. In this paper we will write the vector of independent variables as $\mathbf{q} \in \mathbb{R}^{n_\mathbf{q}}$, where the number of DOF is denoted $n_\mathbf{q}$. The time derivative of the independent variables will be contained in the vector $\mathbf{s} \in \mathbb{R}^{n_\mathbf{q}}$.

2.2 Newton-Euler Equations of Motion with Eliminated Constraints

[10] gives the Newton-Euler Equations of Motion with Eliminated Constraint Forces (NE-EC) as:

$$\begin{aligned} &\sum_{k=1}^{N} \left[\left(\frac{\partial \mathbf{v}_{c_k}^{b_k}}{\partial \mathbf{s}} \right)^\top \left(m_k \dot{\mathbf{v}}_{c_k}^{b_k} + m_k \mathbf{S}(\boldsymbol{\omega}_{nb_k}^{b_k}) \mathbf{v}_{c_k}^{b_k} \right) \right] + \\ &\sum_{k=1}^{N} \left[\left(\frac{\partial \boldsymbol{\omega}_{nb_k}^{b_k}}{\partial \mathbf{s}} \right)^\top \left(\mathbf{I}_{c_k} \dot{\boldsymbol{\omega}}_{nb_k}^{b_k} + \mathbf{S}(\boldsymbol{\omega}_{nb_k}^{b_k}) \mathbf{I}_{c_k} \boldsymbol{\omega}_{nb_k}^{b_k} \right) \right] \\ = &\sum_{k=1}^{N} \left[\left(\frac{\partial \mathbf{v}_{c_k}^{b_k}}{\partial \mathbf{s}} \right)^\top \mathbf{f}_{c_k}^{b_k} + \left(\frac{\partial \boldsymbol{\omega}_{nb_k}^{b_k}}{\partial \mathbf{s}} \right)^\top \mathbf{m}_{c_k}^{b_k} \right] \end{aligned} \quad (1)$$

where:

- n represents the inertial ned-frame, also termed the north-east-down coordinate frame.
- k is the number of the body under consideration, in a system of N bodies
- $\mathbf{v}_{c_k}^{b_k}$ is the linear velocity of the center of gravity c_k of body k, expressed in the b_k-frame, i.e. the body-fixed frame in body k.
- $\boldsymbol{\omega}_{nb_k}^{b_k}$ is the angular velocity of the body-fixed b_k-frame about the inertial n-frame, expressed in the b_k-frame.
- $\mathbf{f}_{c_k}^{b_k}$ and $\mathbf{m}_{c_k}^{b_k}$ are the external forces and moments acting on and about the center of gravity of each body.
- $\frac{\partial \mathbf{v}_{c_k}^{b_k}}{\partial \mathbf{s}}$ is known as the *partial linear velocity* for body k.
- $\frac{\partial \boldsymbol{\omega}_{nb_k}^{b_k}}{\partial \mathbf{s}}$ is known as the *partial angular velocity* for body k.
- m_k is the mass of body k and $\mathbf{I}_{c_k}$ is the inertia matrix of body k, about its center of gravity c_k.
- the skew symmetric matrix $\mathbf{S}$ is the matrix algebra equivalent to the cross product, e.g., $\mathbf{S}(\boldsymbol{\omega})\mathbf{r} = \vec{\omega} \times \vec{r}$.

Our goal is to express Equation 1 in a somewhat more compact form. To this end, we begin by defining the *velocity transformation matrix* $\mathbf{P} \in \mathbb{R}^{n_\mathbf{q} \times 6N}$:

$$\mathbf{P} = \left[\left(\frac{\partial \mathbf{v}_{c_1}^{b_1}}{\partial \mathbf{s}} \right)^\top, \left(\frac{\partial \boldsymbol{\omega}_{nb_1}^{b_1}}{\partial \mathbf{s}} \right)^\top, ... \right. \\ \left. , ..., \left(\frac{\partial \mathbf{v}_{c_N}^{b_N}}{\partial \mathbf{s}} \right)^\top, \left(\frac{\partial \boldsymbol{\omega}_{nb_N}^{b_N}}{\partial \mathbf{s}} \right)^\top \right] \quad (2)$$

A useful formulation results from noticing [11]:

$$\begin{bmatrix} m_k \dot{\mathbf{v}}_{c_k}^{b_k} + m_k \mathbf{S}(\boldsymbol{\omega}_{nb_k}^{b_k}) \mathbf{v}_{c_k}^{b_k} \\ \mathbf{I}_{c_k} \dot{\boldsymbol{\omega}}_{nb_k}^{b_k} + \mathbf{S}(\boldsymbol{\omega}_{nb_k}^{b_k}) \mathbf{I}_{c_k} \boldsymbol{\omega}_{nb_k}^{b_k} \end{bmatrix} = \mathbf{M}_{RB}^{b_k} \dot{\boldsymbol{\nu}}_k + \mathbf{C}_{RB}^{b_k} \boldsymbol{\nu}_k \quad (3)$$

where $\boldsymbol{\nu}_k = [\mathbf{v}_{c_k}^{b_k\top}, \boldsymbol{\omega}_{nb_k}^{b_k\top}]^\top$. In addition, $\mathbf{M}_{RB}^{b_k} \in \mathbb{R}^{6\times6}$, the rigid-body inertia matrix of body k, is unique and satisfies:

$$\mathbf{M}_{RB}^{b_k} = \mathbf{M}_{RB}^{b_k\top} > 0, \qquad \dot{\mathbf{M}}_{RB}^{b_k} = \mathbf{0}_{6\times6}$$

$$\mathbf{M}_{RB}^{b_k} = \begin{bmatrix} m_k \mathbf{I}_{3\times3} & \mathbf{0}_{3\times3} \\ \mathbf{0}_{3\times3} & \mathbf{I}_{c_k} \end{bmatrix} \quad (4)$$

and $\mathbf{C}_{RB}^{b_k}(\boldsymbol{\nu}_k) \in \mathbb{R}^{6\times6}$ is the non-unique Coriolis-Centripetal matrix. One instance where $\mathbf{C}_{RB}^{b_k}(\boldsymbol{\nu}_k)$ is *skew-symmetric* is as follows [11]:

$$\mathbf{C}_{RB}^{b_k}(\boldsymbol{\nu}_k) = \begin{bmatrix} \mathbf{0}_{3\times3} & -m_k \mathbf{S}(\mathbf{v}_{c_k}^{b_k}) \\ -m_k \mathbf{S}(\mathbf{v}_{c_k}^{b_k}) & -\mathbf{S}(\mathbf{I}_{c_k} \boldsymbol{\omega}_{nb_k}^{b_k}) \end{bmatrix} \quad (5)$$

Further, we write the generalised velocities $\boldsymbol{\nu} = [\boldsymbol{\nu}_1^\top, ..., \boldsymbol{\nu}_N^\top]^\top$ in terms of $\mathbf{s}$, the independent velocities:

$$\boldsymbol{\nu} = \mathbf{P}^\top \mathbf{s} \quad (6)$$

and hence:

$$\dot{\boldsymbol{\nu}} = \mathbf{P}^\top \dot{\mathbf{s}} + \dot{\mathbf{P}}^\top \mathbf{s} \quad (7)$$

Drawing on Equations 1, 2, 3, 6 and 7, we arrive at the following result:

$$\mathbf{M}_{RB}^{g} \dot{\mathbf{s}} + \mathbf{C}_{RB}^{g}(\mathbf{q}, \mathbf{s}) \mathbf{s} = \boldsymbol{\tau}_{RB}^{g} \quad (8)$$

where $\mathbf{M}_{RB}^{g} \in \mathbb{R}^{n_\mathbf{q} \times n_\mathbf{q}}$ is the generalised mass matrix for the $n_\mathbf{q}$ DOF multibody system, given by:

$$\mathbf{M}_{RB}^{g} = \mathbf{P} \mathbf{M}_{RB}^{b} \mathbf{P}^\top \quad (9)$$

where $\mathbf{M}_{RB}^{b} \in \mathbb{R}^{6N \times 6N} = diag(\mathbf{M}_{RB}^{b_1} ... \mathbf{M}_{RB}^{b_N})$.
Also we have defined $\mathbf{C}_{RB}^{g}(\mathbf{q}, \mathbf{s}) \in \mathbb{R}^{n_\mathbf{q} \times n_\mathbf{q}}$, the generalised Coriolis-Centripetal matrix for the $n_\mathbf{q}$ DOF multibody system, given by:

$$\mathbf{C}_{RB}^{g}(\mathbf{q}, \mathbf{s}) = \mathbf{P} \mathbf{M}_{RB}^{b} \dot{\mathbf{P}}^\top + \mathbf{P} \mathbf{C}_{RB}^{b}(\boldsymbol{\nu}) \mathbf{P}^\top \quad (10)$$

where $\mathbf{C}_{RB}^{b} \in \mathbb{R}^{6N \times 6N} = diag\left(\mathbf{C}_{RB}^{b_1}(\boldsymbol{\nu}) ... \mathbf{C}_{RB}^{b_N}(\boldsymbol{\nu}) \right)$.
On the right hand side of Equation 8, we have defined $\boldsymbol{\tau}_{RB}^{g} \in \mathbb{R}^{n_\mathbf{q}}$, given by:

$$\boldsymbol{\tau}_{RB}^{g} = \mathbf{P} \boldsymbol{\tau}_{RB}^{b} \quad (11)$$

where $\boldsymbol{\tau}_{RB}^{b} \in \mathbb{R}^{6N} = [\boldsymbol{\tau}_{RB}^{b_1\top} ... \boldsymbol{\tau}_{RB}^{b_N\top}]^\top$ and $\boldsymbol{\tau}_{RB}^{b_k} = [\mathbf{v}_{c_k}^{b_k\top}, \boldsymbol{\omega}_{nb_k}^{b_k\top}]^\top$

2.3 External Forces

Fossen [12] gives the external forces (as opposed to internal hinge forces) acting on a single surface vessel as:

$$\boldsymbol{\tau}_{RB}^{b_k} = -\mathbf{M}_A^{b_k}\dot{\boldsymbol{\nu}}_k - \boldsymbol{\mu}_k - \mathbf{G}^{b_k}\boldsymbol{\eta}_k^{b_k} + \boldsymbol{\tau}_E^{b_k} + \boldsymbol{\tau}^{b_k} \quad (12)$$

where $\mathbf{M}_A^{b_k} \in \mathbb{R}^{6\times6}$ is the added inertia matrix, $\mathbf{G}^{b_k} \in \mathbb{R}^{6\times6}$ is the hydrostatic restoring matrix, and $\boldsymbol{\tau}^{b_k} \in \mathbb{R}^6$ is the control force acting on body k. Further, the wave-excitation forces $\boldsymbol{\tau}_E^{b_k} \in \mathbb{R}^6$ are composed of:

$$\boldsymbol{\tau}_E^{b_k} = \boldsymbol{\tau}_{FK}^{b_k} + \boldsymbol{\tau}_D^{b_k} \quad (13)$$

where:

$$\begin{aligned} \boldsymbol{\tau}_{FK}^{b_k} &= \text{generalised (Cartesian) Froude-Krylov forces} \\ \boldsymbol{\tau}_D^{b_k} &= \text{generalised (Cartesian) Diffraction forces} \end{aligned}$$

The $\boldsymbol{\mu}_k$ represents the convolution integral term in Cummins equation. Here a state-space approximation to the convolution integral is applied [13]. The overall state space model for the single vessel is thus given by:

$$\begin{aligned} \dot{\boldsymbol{\eta}}_k &= \mathbf{J}^{b_k}\boldsymbol{\nu}_k \quad (14) \\ \mathbf{M}^{b_k}\dot{\boldsymbol{\nu}}_k + \mathbf{C}_{RB}^{b_k}(\boldsymbol{\nu})\boldsymbol{\nu} + \boldsymbol{\mu}_k + \mathbf{G}^{b_k}\boldsymbol{\eta}_k^{b_k} &= \boldsymbol{\tau}_E^{b_k} + \boldsymbol{\tau}^{b_k} \\ \dot{\boldsymbol{\chi}}_k = \mathbf{A}_\mathbf{r}\boldsymbol{\chi}_k &+ \mathbf{B}_\mathbf{r}\boldsymbol{\nu}_k \quad (15) \\ \boldsymbol{\mu}_k = \mathbf{C}_\mathbf{r}\boldsymbol{\chi}_k &+ \mathbf{D}_\mathbf{r}\boldsymbol{\nu}_k \quad (16) \end{aligned}$$

where $\boldsymbol{\chi}_k(0) = \mathbf{0}$.
Utilising Equations 11, 6 and 7, it becomes possible to extend the state-space model (Equations 14:16) to N interconnected surface vessels:

$$\begin{aligned} \dot{\mathbf{q}} &= \mathbf{s} \quad (17) \\ \mathbf{M}^g\dot{\mathbf{s}} + \mathbf{C}_{RB}^g(\mathbf{q},\mathbf{s})\dot{\mathbf{s}} + \boldsymbol{\mu} + \mathbf{G}^b\mathbf{q} &= \boldsymbol{\tau}_E^g + \boldsymbol{\tau}_c^g \quad (18) \\ \dot{\boldsymbol{\chi}}_k = \mathbf{A}_\mathbf{r}^{\mathbf{b_k}}\boldsymbol{\chi}_k &+ \mathbf{B}_\mathbf{r}^{\mathbf{b_k}}\boldsymbol{\nu}_k \quad (19) \\ \boldsymbol{\mu}_k^{b_k} = \mathbf{C}_\mathbf{r}^{\mathbf{b_k}}\boldsymbol{\chi}_k &+ \mathbf{D}_\mathbf{r}^{\mathbf{b_k}}\boldsymbol{\nu}_k \quad (20) \end{aligned}$$

where $\mathbf{M}^b \in \mathbb{R}^{6N\times6N} = \mathbf{M}_{RB}^b + \mathbf{M}_A^b$ and $\mathbf{M}^g \in \mathbb{R}^{n_\mathbf{q}\times n_\mathbf{q}}$ is given by:

$$\mathbf{M}^g = \mathbf{P}\mathbf{M}^b\mathbf{P}^\top \quad (21)$$

and $\mathbf{G}^g \in \mathbb{R}^{n_\mathbf{q}\times n_\mathbf{q}}$ is given by:

$$\mathbf{G}^g = \mathbf{P}\mathbf{G}^b\mathbf{P}^\top \quad (22)$$

where $\mathbf{G}^b \in \mathbb{R}^{6N\times6N}$ is given by:

$$\mathbf{G}^b = diag(\mathbf{G}^{b_1}, ..., \mathbf{G}^{b_k}, ..., \mathbf{G}^{b_N}) \quad (23)$$

and $\mathbf{G}^{b_k} \in \mathbb{R}^{6\times6}$ is given by:

$$\mathbf{G}^{b_k} = diag(0, 0, \rho g A_{WP}(0), \rho g \nabla\overline{GM}_T, \rho g \nabla\overline{GM}_L) \quad (24)$$

Finally, we note that

$$\boldsymbol{\mu}^g = \mathbf{P}\boldsymbol{\mu}^b \quad (25)$$

where: $\boldsymbol{\mu}^b \in \mathbb{R}^{6N} = [\boldsymbol{\mu}_k^{b_k\top}, ..., \boldsymbol{\mu}_N^{b_N\top}]^\top$,

2.4 Hydrodynamics

A hydrodynamic software package with multibody functionality (such as WAMIT), may be used to obtain added mass and radiation damping coefficients. For example, the added mass matrix for a *two-body* system given by WAMIT is $\mathbf{A}(\omega) \in \mathbb{R}^{12\times12}$. With some transformations, detailed below, it becomes possible to incorporate the $6N \times 6N$ added mass and radiation damping matrices into the model developed in Section 3.1. This is a significant advantage of the method presented.

The radiation damping matrix for frequency ω is given by $\mathbf{B}(\omega) \in \mathbb{R}^{6N\times6N}$. Following frequency- to time-domain processing discussed in Section 2.3 above, the resulting $6N$ force vector $\boldsymbol{\mu}_k$, expressed in the b_k-frame, is easily incorporated using the velocity transformation matrix $\mathbf{P}$ (Equation 11).

All quantities output by WAMIT are expressed in a Cartesian data frame with origin on the free surface in the same vertical line as the center of gravity, as shown in Figure 2.4.

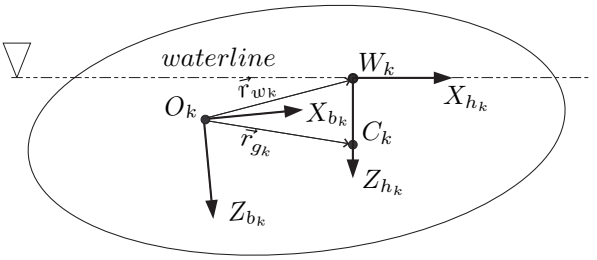

Figure 1: Definitions of coordinate origins on body k: W_k (waterline), C_k (centre of gravity) and O_k (equations of motion). The h_k-frame is located in W_k and the b_k-frame is located in O_k

Hence it is necessary utilise the following transform, given in [12]:

$$\mathbf{T}_{data_k}^{h_k} = \begin{bmatrix} \mathbf{R}_{data_k}^{h_k} & 0 \\ 0 & \mathbf{R}_{data_k}^{h_k} \end{bmatrix} \quad (26)$$

where:

$$\mathbf{R}_{data_k}^{h_k} = \begin{bmatrix} 1 & 0 & 0 \\ 0 & -1 & 0 \\ 0 & 0 & -1 \end{bmatrix} \quad (27)$$

It now becomes necessary to transform the quantities above expressed in the h_k-frame into the b_k-frame. The $\mathbf{J}^{h_k}$ transform converts quantities from the coordinate frames used in hydrodynamic software to the body-fixed frames convenient for control modeling. We assume that the oscillations $\delta\boldsymbol{\Theta}_k$ of the b_k-frame about the h_k-frame are given by the tranform[14]:

$$\mathbf{J}^{h_k}(\delta\boldsymbol{\Theta}_k) = \begin{bmatrix} \mathbf{R}_{b_k}^{h_k}(\delta\boldsymbol{\Theta}_k) & \mathbf{0}_{3\times3} \\ \mathbf{0}_{3\times3} & \mathbf{R}_{b_k}^{h_k}(\delta\boldsymbol{\Theta}_k) \end{bmatrix} \mathbf{H}(\mathbf{r}_{w_k}^{b_k}) \quad (28)$$

where $\delta\boldsymbol{\Theta}_k$ signifies small angles, and $\mathbf{R}_{b_k}^{h_k}(\delta\boldsymbol{\Theta}_k) \in SO(3)$ is given by:

$$\mathbf{R}_{b_k}^{h_k}(\delta\boldsymbol{\Theta}_k) = \begin{bmatrix} 1 & -\delta\psi & \delta\theta \\ \delta\psi & 1 & -\delta\phi \\ -\delta\theta & \delta\phi & 1 \end{bmatrix} \quad (29)$$

and we have assumed $\dot{\mathbf{J}}^{h_k}(\delta\boldsymbol{\Theta}_k) \approx \mathbf{0}_{6\times6}$.

For many applications, the roll, pitch and yaw oscillations of the b_k-frame with respect to the h_k-frame, $\delta\phi_k, \delta\theta_k$ and $\delta\psi_k$, will be small, such that:

$$\mathbf{R}_{b_k}^{h_k}(\delta\boldsymbol{\Theta}_k) \approx \mathbf{I}_{3\times 3} \tag{30}$$

and:

$$\mathbf{J}^{h_k}(\delta\boldsymbol{\Theta}_k) \overset{\delta\boldsymbol{\Theta} \text{ small}}{\approx} \mathbf{H}(\mathbf{r}_{w_k}^{b_k}) \tag{31}$$

The necessary transform, fully derived in [14], may be stated here as:

$$\boldsymbol{\tau}^{h_k} = \mathbf{J}^{h_k}(\delta\boldsymbol{\Theta}_k)\boldsymbol{\tau}^{b_k} \tag{32}$$

3 Example: Two-Body Marine System

Wave-tank experiments were carried out on the hinged-barge wave-energy system shown in Figure 2. A series of static, decay,

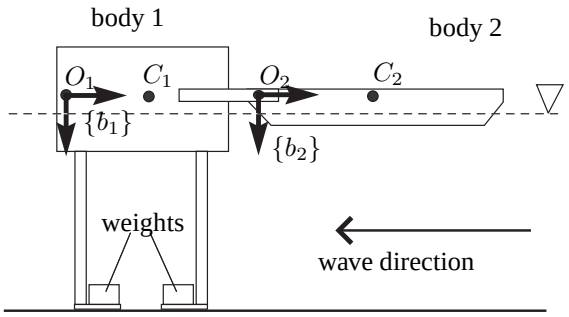

Figure 2: Two-body hinged-barge system, where $\{b_1\}$ and $\{b_2\}$ indicate the b-frames of bodies one and two, respectively.

regular and irregular wave tests were conducted on the device. Full details are documented in [15].

3.1 Rigid Body Dynamics

$$\mathbf{r}_{o_2}^{b_1} = [L_{o_2}, 0, 0]^\top \tag{33}$$

$$\mathbf{r}_{c_1}^{b_1} = [L_{c_1}, 0, 0]^\top \qquad \mathbf{r}_{c_2}^{b_2} = [L_{c_2}, 0, 0]^\top \tag{34}$$

$$\boldsymbol{\omega}_{nb_1}^{b_1} = [0, \theta_1, 0]^\top \qquad \boldsymbol{\omega}_{nb_2}^{b_2} = [0, \theta_2, 0]^\top \tag{35}$$

$$\dot{\boldsymbol{\omega}}_{nb_1}^{b_1} = [0, \dot{\theta_1}, 0]^\top \qquad \dot{\boldsymbol{\omega}}_{nb_2}^{b_2} = [0, \dot{\theta_2}, 0]^\top \tag{36}$$

$$\mathbf{v}_{c_1}^{b_1} = \mathbf{v}_{o_1}^{b_1} + \boldsymbol{\omega}_{nb_1}^{b_1} \times \mathbf{r}_{c_1}^{b_1} \tag{37}$$

$$= \mathbf{S}(\boldsymbol{\omega}_{nb_1}^{b_1})\mathbf{r}_{c_1}^{b_1} \tag{38}$$

$$= [0, 0, -L_{c_1}\dot{\theta}_1]^\top \tag{39}$$

$$\mathbf{v}_{c_2}^{b_2} = \mathbf{v}_{o_2}^{b_2} + \boldsymbol{\omega}_{nb_2}^{b_2} \times \mathbf{r}_{c_2}^{b_2} \tag{40}$$

$$= \mathbf{R}_{b_1}^{b_2}(\boldsymbol{\omega}_{nb_1}^{b_1} \times \mathbf{r}_{o_1}^{b_1}) + \boldsymbol{\omega}_{nb_2}^{b_2} \times \mathbf{r}_{c_2}^{b_2} \tag{41}$$

$$= \mathbf{R}_{b_1}^{b_2}\mathbf{S}(\boldsymbol{\omega}_{nb_1}^{b_1})\mathbf{r}_{o_1}^{b_1} + \mathbf{S}(\boldsymbol{\omega}_{nb_2}^{b_2})\mathbf{r}_{c_2}^{b_2} \tag{42}$$

$$= [L_1 s_{21}\dot{\theta}_1, 0, -L_1 c_{21}\dot{\theta}_1 - L_{c_1}\dot{\theta}_1]^\top \tag{43}$$

where where we have defined $c_{21} = \cos(\theta_2 - \theta_1)$, $s_{21} = \sin(\theta_2 - \theta_1)$, and the rotation matrix $R_{b_1}^{b_2}$ describing rotations, in the $x-z$ plane, of the b_2-frame about the b_1-frame is given by:

$$\mathbf{R}_{b_1}^{b_2} = \mathbf{R}_{b_2}^{b_1\,-1} = \mathbf{R}_{b_2}^{b_1\,\top} \tag{44}$$

$$= \begin{bmatrix} c_{21} & 0 & -s_{21} \\ 0 & 1 & 0 \\ s_{21} & 0 & s_{21} \end{bmatrix} \tag{45}$$

Now we choose $\mathbf{q} = [\theta_1, \theta_2]^\top$. Hence $\mathbf{s} = [\dot{\theta}_1, \dot{\theta_2}]^\top$, and it follows that:

$$\frac{\partial \mathbf{v}_{c_1}^{b_1}}{\partial \mathbf{s}} = \begin{bmatrix} 0 & 0 \\ 0 & 0 \\ -Lc_1 & 0 \end{bmatrix} \tag{46}$$

$$\frac{\partial \mathbf{v}_{c_2}^{b_2}}{\partial \mathbf{s}} = \begin{bmatrix} L_1 s_{21} & 0 \\ 0 & 0 \\ -L_1 c_{21} & -L_{c_2} \end{bmatrix} \tag{47}$$

Also:

$$\frac{\partial \boldsymbol{\omega}_{nb_1}^{b_1}}{\partial \mathbf{s}} = \begin{bmatrix} 0 & 0 \\ 1 & 0 \\ 0 & 0 \end{bmatrix}, \quad \frac{\partial \boldsymbol{\omega}_{nb_2}^{b_2}}{\partial \mathbf{s}} = \begin{bmatrix} 0 & 0 \\ 0 & 1 \\ 0 & 0 \end{bmatrix} \tag{48}$$

This gives the *partial velocity matrix* $\mathbf{P} \in \mathbb{R}^{2\times 12}$ as:

$$\mathbf{P} = \begin{bmatrix} 0 & 0 & -Lc_1 & 0 & 1 & 0 & & & & & & \\ 0 & 0 & 0 & 0 & 0 & 0 & & & & & & \\ & & & & & & L_1 s_{21} & 0 & -L_1 c_{21} & 0 & 0 & 0 \\ & & & & & & 0 & 0 & -L_{c_2} & 0 & 1 & 0 \end{bmatrix} \tag{49}$$

From Equations 9 and 10 the following expression for $\mathbf{M}_{RB}^g \in \mathbb{R}^{2\times 2}$ and $\mathbf{C}_{RB}^g(\mathbf{q}, \mathbf{s}) \in \mathbb{R}^{2\times 2}$ may be calculated:

$$\mathbf{M}_{RB}^g = \begin{bmatrix} I_{1y} + m_1 L_{c_1}^2 + m_2 L_1^2 & m_2 L_1 L_{c_2} c_{21} \\ m_2 L_1 L_{c_2} c_{21} & I_{2y} + m_2 L_{c_2}^2 \end{bmatrix} \tag{50}$$

$$\mathbf{C}_{RB}^g(\mathbf{q}, \mathbf{s}) = \begin{bmatrix} 0 & -m_2 L_1 L_{c_2} s_{21}\dot{\theta}_2 \\ m_2 L_1 L_{c_2} s_{21}\dot{\theta}_1 & 0 \end{bmatrix} \tag{51}$$

3.2 Hydrodynamics

Using the state-space approximation of [13] for the convolution term in the Cummins equation [16], we find:

$$\mu_1^{b_1} = \sum_i \mu_{1,i} \qquad i = 1, 3, 5, 7, 9, 11 \tag{52}$$

$$\mu_3^{b_1} = \sum_i \mu_{3,i} \qquad i = 1, 3, 5, 7, 9, 11 \tag{53}$$

$$\mu_5^{b_1} = \sum_i \mu_{5,i} \qquad i = 1, 3, 5, 7, 9, 11 \tag{54}$$

$$\mu_7^{b_2} = \sum_i \mu_{7,i} \qquad i = 1, 3, 5, 7, 9, 11 \tag{55}$$

$$\mu_9^{b_2} = \sum_i \mu_{9,i} \qquad i = 1, 3, 5, 7, 9, 11 \tag{56}$$

$$\mu_{11}^{b_2} = \sum_i \mu_{11,i} \qquad i = 1, 3, 5, 7, 9, 11 \tag{57}$$

$$\boldsymbol{\mu}^b = \Big[\mu_1^{b_1}, 0, \mu_3^{b_1}, 0, \mu_5^{b_1}, 0, \mu_7^{b_2}, 0, \mu_9^{b_2}, 0, \mu_{11}^{b_2}, 0\Big]^\top \tag{58}$$

Hence $\boldsymbol{\mu}^g \in \mathbb{R}^{2\times 2}$ is given by:

$$\boldsymbol{\mu}^g = \mathbf{P}\boldsymbol{\mu}^b \tag{59}$$

Satisfactory agreement with the impulse response functions are achieved using an Order 6 state-space model of the convolution integral term.
$\mathbf{A}(\infty)$ is taken at the highest value of ω calculated, i.e. $\omega = 12$ rad/s. This is a somewhat crude approximation (a more formal method is given in [17]); however the weakness of the state-space approximation approach, such as that of [13] used here, is that good values for $\mathbf{A}(\infty)$ are difficult to obtain. This is due to the need for ever smaller panel sizes as frequency increases, and hence prohibitively long run-times. The method presented in [18] overcomes the need for added-mass at infinite frequency calculations. It is reasonably straightforward to incorporate the latter model for radiation forces into the approach presented in this paper.

Using the hydrostatic restoring matrix expression of 22 we find $\mathbf{G}^g \in \mathbb{R}^{2\times 2}$:

$$\mathbf{G}^g = \begin{bmatrix} L_{c1}^2 A_{\text{WP}_1}(0) + L_1^2 A_{\text{WP}_2}(0) + \nabla_1 G M_{L_1} & L_1 L_{c_2} A_{\text{WP}_2}(0) \\ L_1 L_{c_2} A_{\text{WP}_2}(0) & L_{c_2}^2 A_{\text{WP}_2}(0) + \nabla_2 G M_{L_2} \end{bmatrix} \quad (60)$$

With reference to expressions developed in this sections, we write the state-space model of the two-body system as follows:

$$\dot{\mathbf{q}} = \mathbf{s} \quad (61)$$

$$\mathbf{M}^g \dot{\mathbf{s}} + \mathbf{C}_{RB}^g(\mathbf{q},\mathbf{s})\dot{\mathbf{s}} + \boldsymbol{\mu} + \mathbf{G}^g = \boldsymbol{\tau}_E^g + \boldsymbol{\tau}^g \quad (62)$$

$$\dot{\boldsymbol{\chi}} = \mathbf{A}_\mathbf{r}^\mathbf{b}\boldsymbol{\chi} + \mathbf{B}_\mathbf{r}^\mathbf{b}\boldsymbol{\nu} \quad (63)$$

$$\boldsymbol{\mu}^b = \mathbf{C}_\mathbf{r}^\mathbf{b}\boldsymbol{\chi} + \mathbf{D}_\mathbf{r}^\mathbf{b}\boldsymbol{\nu} \quad (64)$$

where $\mathbf{M}^g \in \mathbb{R}^{2\times 2}$ and $\boldsymbol{\tau}^g \in \mathbb{R}^2$ are given by:

$$\mathbf{M}^g = \mathbf{M}_{RB}^g + \mathbf{M}_A^g \quad (65)$$

$$\boldsymbol{\tau}^g = \boldsymbol{\tau}_{PTO}^g + \boldsymbol{\tau}_{moor}^g + \boldsymbol{\tau}_{hinge}^g \quad (66)$$

4 Validation Against Experimental Results

In experiments, regular head waves excited the *two-body* system shown in Figure 2. Waves of height $H = 60mm$ over a range of 14 frequencies were applied, with the heave response of body two in ned-coordinates recorded over this interval. The response of the model derived in Sections 3.1 and 3.2 is simulated over the same frequency range. Certain model parameters were known from the experiments. In order to determine the unknown model parameters, an optimisation algorithm using the simplex search method of [19] was applied. This is a direct search method that does not use numerical or analytic gradients. The objective function minimised calculated the sum of the squared distances between corresponding points on the experiments and simulations, *i.e.*,

$$error = \sum_{i=1}^{N} |\hat{f}_i - f_i|^2 \quad (67)$$

where $\hat{f}_i$ is element i in the vector of peaks and lows in the experimental measurements and f_i is corresponding element in the vector of peaks and lows from simulated measurements. Note that N is the number of peaks and lows for the measurements being compared. The optimisation comprises a least-squares fit of simulations to experiments across all measured frequencies. Consequently, an overall mean squared error (MSE) across all frequencies was determined:

$$MSE = 8.86 \quad \text{mm}^2$$

As a reference, the maximum amplitude considered is approximately 25 mm, and the minimum is approximately 8 mm. Figure 3 gives a comparison of the simulated to experimental frequency response of the heave of body two.

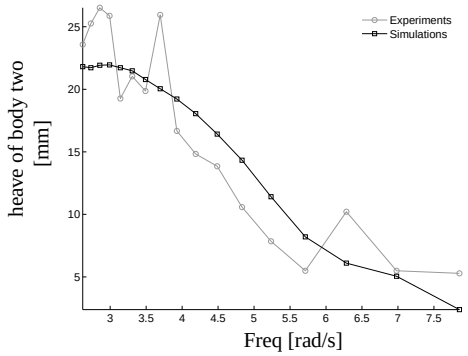

Figure 3: Frequency response of the heave of body two for experiments and simulations

Figure 4 shows the response in heave of body two for a frequency of $\omega = 3.3$ rad/s.

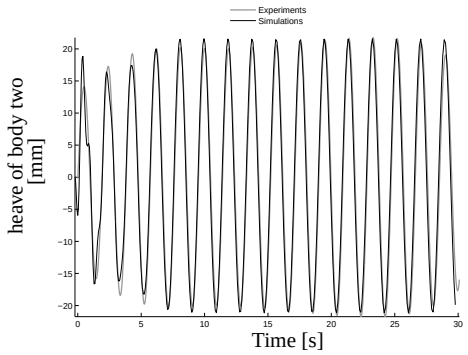

Figure 4: Comparison of Body 2 heave response to regular wave excitation of height $H = 60$ mm and $\omega = 3.3$ rad/s

Figure 5 shows the response in heave of body two for a frequency of $\omega = 7$ rad/s. The oscillatory envelope in the experiments are deemed to be due to unmodelled dynamics.

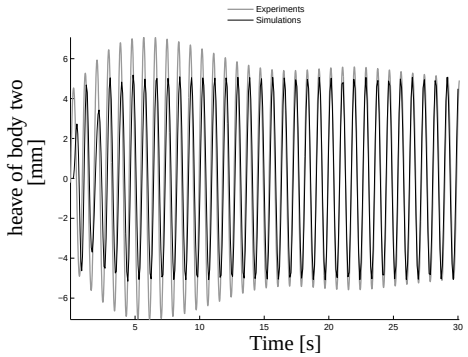

Figure 5: Comparison of Body 2 heave response to regular wave excitation of height $H = 60$ mm and $\omega = 7$ rad/s

5 Conclusions

The modelling approach presented in this paper is:

- Useful for simulation: The models derived using this method are easily implemented in Simulink®. Various configurations of marine multibody systems may be conveniently tested by adjusting distance parameters between simulations. Control designs may be tested within such a simulation environment, which provides a detailed description of the actual physical process. The accuracy of this so-called *process-plant model* is currently limited to linear motions, which for a large number of multibody marine systems may be considered normal operating conditions.
- Useful for control design: The Fossen formulation of the modelling approach presented implies suitability for system analysis and control design. System properties evident in matrix components of the system equations of motion may be exploited when doing control design. Additionally, process-plant models in the Fossen formulation are conducive to simplification; such simplified mathematical descriptions, usually linear, containing only the main physical properties of the actual process, are often called *control-plant models*, and are used for development of state-estimators and controllers.
- Useful for wave-energy device modelling: The modelling approach presented gives accurate time-domain models; time-domain modelling of wave-energy devices is particularly important due to the need for information on the device's transient response characteristics. Modelling of a line-absorber has been demonstrated in this paper as well as in [15, 20], while modelling of a four DOF point-absorber is treated in [15]. Complex PTO systems with many moving parts may be integrated conveniently due to the extendable nature of the modelling approach. Additionally, farms of devices can be modelled, with individual device motions referred to the same inertial n-frame.

Further improvements should be made to the treatment of hydrodynamic loads: an analysis of which nonlinear hydrodynamics effects become dominant in various operating conditions is required, followed by development of approximate models incorporating them into models already developed using the approach presented. In addition, improved modelling of nonlinearities in PTO and mooring subsystems is required.

Acknowledgement

The first author would like to thank Jon Vidar Holm of Statoil for his help with the optimisation discussed herein.

References

[1] K. Budal. Theory for absorption of wave power by a system of interacting bodies. *Journal of Ship Research*, 21(248-253.), 1977.

[2] J. Falnes. Radiation impedance matrix and optimum power absorption for interacting oscillatiors in surface waves. *Applied Ocean Research*, 2:75–80., 1980.

[3] 1-25. M.J. Simon Journal of Fluid Mechanics, Vol. 120. Multiple scattering in arrays of axisymmetric wave-energy devices. part 1. a matrix method using a plane-wave approximation. *Journal of Fluid Mechanics*, 120:1–25.

[4] P. McIver. Wave forces on adjacent floating bridges. *Applied Ocean Research*, 8:67–75, 1986.

[5] D.V. Evans. Some analytic results for two and three dimensional wave-energy absorbers. *Power from Sea Waves (edited by B. Count), Academic Press*, pages 213–249, 1980.

[6] D.R.B. Kraemer. *The Motions of Hinged-Barge Systems in Regular Seas*. PhD thesis, Johns Hopkins University, 2000.

[7] P.I. Berntsen. Configuration control and motion damping of single point anchored interconnected marine structures. Masters thesis, Dept. Marine Hydrodynamics, NTNU, Trondheim, NORWAY, 2002.

[8] SNAME. The society of naval architects and marine engineers. nomenclature for treating the motion of a submerged body through a fluid. *Technical and Research Bulletin*, (1-5), 1950.

[9] A. Shabana. *Dynamics of Multibody Systems*. Cambridge, 3rd edition, 2005.

[10] O. Egeland and J.T. Gravdahl. *Modeling and Simulation for Automatic Control*. Marine Cybernetics, 2002.

[11] Thor I. Fossen. *Marine Control Systems: Guidance,Navigation, and Control of Ships, Rigs and Underwater Vehicles*. Marine Cybernetics, 2002.

[12] T.I. Fossen. A nonlinear unified state-space model for ship maneuvering and control in a seaway. *Journal of Bifurication and Chaos*, September 2005.

[13] E. Kristiansen and O. Egeland. Frequency-dependant added mass in models for controller design for wave motion damping. In *Proc.6th MCMC*, Girona, Spain, 2003.

[14] T.I. Fossen and Ø. Smøgeli. Nonlinear time-domain strip theory formulation for low-speed maneuvering and station-keeping. *Modelling,Identification and Control*, 25(4):201–221, 2004.

[15] M. Ó'Catháin. Modelling of multibody marine systems with application to wave-energy devices. Mengsc thesis, Dept. Electronic Engineering, NUI Maynooth, Maynooth, Co. Kildare, IRELAND, May 2007.

[16] W.E. Cummins. The impulse response function and ship motions. *Technical Report 1661. David Taylor Model BasinDTNSRDC.*, 1962.

[17] M. Greenhow. A note on the high frequency limits of a floating body. *J. Ship Res.*, 28:226–228, 1984.

[18] T. Perez and O. Lande. A frequency-domain approach to modeling and identification of the force to motion vessel response. In *7th IFAC Conference on Manoeuvring and Control of Marine Vessels MCMC*, Portugal, Sept 2006.

[19] J.C. Lagarias, J. A. Reeds, M. H. Wright, and P. E. Wright. Convergence properties of the nelder-mead simplex method in low dimensions. *SIAM Journal of Optimisation*, 9(1):112–147, 1998.

[20] M. Ó'Catháin, T.I. Fossen, and B.J. Leira. Control-oriented modelling of a 2-body interconnected marine system. In *Proc. 7th MCMC*, Lisbon, Portugal, September 2006.